Quantifying dynamic water storage in unsaturated bedrock with borehole nuclear magnetic resonance

Logan Marcos Schmidt[1] and Daniella Rempe[2]

[1]University of Texas Institute for Geophysics
[2]University of Texas at Austinn

January 20, 2023

Abstract

Quantifying the volume of water that is stored in the subsurface is critical to studies of water availability to ecosystems, slope stability, and water-rock interactions. In a variety of settings, water is stored in fractured and weathered bedrock as rock moisture. However, few techniques are available to measure rock moisture in unsaturated rock, making direct estimates of water storage dynamics difficult to obtain. Here, we use borehole nuclear magnetic resonance (NMR) at two sites in seasonally dry California to quantify dynamic rock moisture storage. We show strong agreement between NMR estimates of dynamic storage and estimates derived from neutron logging and mass balance techniques. The depths of dynamic storage are up to 9 m and likely reflect the depth extent of root water uptake. To our knowledge, these data are the first to quantify the volume and depths of dynamic water storage in the bedrock vadose zone via NMR.

Quantifying dynamic water storage in unsaturated bedrock with borehole nuclear magnetic resonance

Logan Schmidt[1], **Daniella Rempe**[1]

[1]Department of Geological Sciences, Jackson School of Geosciences, University of Texas at Austin, Austin, TX 78701

Key Points:

- Borehole NMR monitoring captures unsaturated water content changes associated with dynamic storage in bedrock fractures.
- Estimates of hillslope dynamic storage derived from borehole NMR, neutron logging, and mass balance techniques agree.
- Borehole NMR and neutron moisture monitoring provide constraints on rooting depth and total water storage.

Corresponding author: Logan Schmidt, `loganmschmidt@utexas.edu`

Abstract

Quantifying the volume of water that is stored in the subsurface is critical to studies of water availability to ecosystems, slope stability, and water-rock interactions. In a variety of settings, water is stored in fractured and weathered bedrock as rock moisture. However, few techniques are available to measure rock moisture in unsaturated rock, making direct estimates of water storage dynamics difficult to obtain. Here, we use borehole nuclear magnetic resonance (NMR) at two sites in seasonally dry California to quantify dynamic rock moisture storage. We show strong agreement between NMR estimates of dynamic storage and estimates derived from neutron logging and mass balance techniques. The depths of dynamic storage are up to 9 m and likely reflect the depth extent of root water uptake. To our knowledge, these data are the first to quantify the volume and depths of dynamic water storage in the bedrock vadose zone via NMR.

Plain Language Summary

Detecting the volume of water stored and exchanged in the subsurface is necessary for understanding water cycling and the transport of nutrients and contaminants. In fractured or weathered bedrock, which underlies a significant fraction of Earth's surface, conventional moisture measurement methods are not readily applied. This study demonstrates that borehole nuclear magnetic resonance (NMR) is a reliable method for quantifying changes in moisture within fractured and weathered bedrock. At two field sites in California, we measure moisture before and after the dry summer growing season with NMR and compare our results to a more conventional neutron moderation technique. We find agreement in the volume of water exchanged and the depths of seasonal water storage.

1 Introduction

Water storage in the unsaturated zone is a fundamental component of the hydrologic cycle that regulates evapotranspiration, runoff, and groundwater recharge. Water storage in soils as soil moisture has received considerable attention, and methodology for quantifying dynamic storage in soils exists across scales (Babaeian et al., 2019). However, less attention has been paid to dynamic storage within fractured bedrock, where dynamic water storage can play a critical role in providing water to vegetation (Schwinning, 2010), dictating the fate of contaminants (Gwo et al., 2005; Faybishenko et al., 2000), and controlling the pace of chemical weathering and biogeochemical cycling (Ireson et al., 2009; Wan et al., 2019). However, few techniques are available to document the spatiotemporal patterns of volumetric water content in unsaturated, fractured bedrock environments.

Nuclear magnetic resonance (NMR) is an emerging geophysical method for estimating the water content and hydraulic properties of the unsaturated zone (Behroozmand et al., 2015). NMR tools are directly sensitive to the hydrogen content of pore fluid and therefore provide robust measurements of volumetric water content. This ability to directly quantify volumetric water content is a distinct advantage of NMR relative to other geophysical methods such as electrical resistivity tomography, seismic, or ground penetrating radar, which are indirectly sensitive to water content. Recently, NMR has been employed to estimate water content in the bedrock vadose zone at the field scale via borehole (e.g. Flinchum et al., 2018; Rempe et al., 2018) and surface (e.g. Carrière et al., 2016; Flinchum et al., 2019; Lesparre et al., 2020) deployments. However, it has not yet been established whether changes in water content, and thus dynamic storage, can be reliably quantified with borehole NMR measurements. The potential limitations of NMR for quantifying changes in water content at the field scale, such as sufficient signal/noise ratio or the presence of minerals with high magnetic susceptibilities (e.g. Keating & Knight, 2008, 2010), have not yet been assessed at the field scale.

Here, we quantify water content changes and dynamic storage in unsaturated bedrock weathering profiles through successive borehole NMR well logging conducted under wet and dry conditions at two seasonally dry field sites. We compare our NMR results to the results of neutron moderation logging and hydrologic mass balance techniques to evaluate borehole NMR as a technique for capturing the magnitude and spatiotemporal patterns of unsaturated dynamic storage in weathered and fractured bedrock.

2 Methods

We exploit two established hillslope study sites—Rivendell and Sagehorn—associated with the Eel River Critical Zone Observatory (ERCZO) in the Northern California Coast Ranges, USA (Figure 1). The sites are approximately 20 km apart. The climate is Mediterranean, with warm dry summers and cool wet winters. Mean annual temperature at the site is 13°C and mean annual precipitation (measured from 1981 to 2010) is 1811 mm

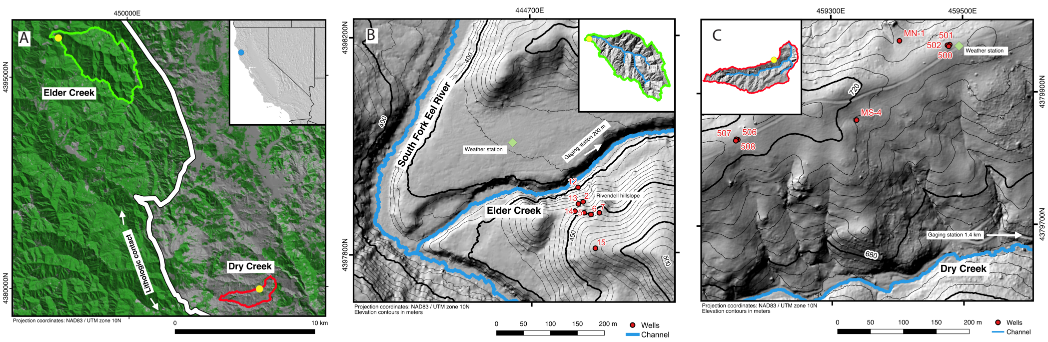

Figure 1. Site maps modified from Dralle et al. (2018). (A) Map of the Elder Creek and Dry Creek watersheds with the locations of Rivendell and Sagehorn shown as yellow dots. The lithologic contact between the Coastal Belt turbidites to the west and the Central Belt mélange to the east is shown as a white line (Jayko et al., 1989). Grey to green pseudocolor represents percent forest (Hansen et al., 2013). Inset shows the state of California with a blue point for the study watersheds location. (B) Bare earth hillshade map of the Rivendell study area. Inset shows the Elder Creek watershed, and the yellow point corresponds to the Rivendell site. Borehole locations are shown as red points. (C) Bare earth hillshade map of the Sagehorn study area. Inset shows the Dry Creek watershed, and the yellow point corresponds to the Sagehorn site. Borehole locations are shown as red points.

(PRISM Climate Group, 2004). The seasonal cumulative precipitation during the 2017 water year was 3381 mm.

Each study site has a distinct lithologic and ecologic setting. The Rivendell site is underlain by turbidites of the Coastal Belt of the Franciscan Formation, consisting of argillite with sandstone and conglomerate interbeds. The Rivendell boreholes (W7, W12, W13, W14, W15, W16) are drilled into the deeply weathered argillite and intersect minor sandstone interbeds. Rivendell hosts a mixed broadleaf needleleaf evergreen forest, and W16 is located on a South facing hillslope where madrone and oaks dominate. The Sagehorn site is underlain by the the Central Belt of the Franciscan Formation, which is a tectonic mélange that consists of tectonically sheared argillite with coherent blocks of varying sizes comprised of different mineralogies. W501 is drilled into argillaceous melange matrix with herbaceous groundcover, while W503 and W505 are drilled into a sandstone block near a mixture of mature bay and live oaks (Hahm et al., 2018).

Boreholes at both sites were drilled and constructed for downhole moisture monitoring. Holes were drilled without water or drilling fluid (via augering or air-rotary coring) and cased snugly with PVC without backfill material (Salve et al., 2012; Hahm et al., 2018). To prevent ponding and short-circuiting of infiltrating water down the borehole, well heads were constructed with outward-sloping concrete. Each borehole penetrates the water table and thus ecompasses the entire length of the unsaturated zone. We conducted two successive logging campaigns during the summer of 2017. Downhole NMR and neutron well logs were conducted in May (wet conditions, high water table) and August and October (dry conditions, low water table, see Table S1).

Borehole NMR logs were acquired with a Dart NMR Logging System (Vista Clara, Inc., Mukilteo, Washington, USA). Measurements were taken every 0.25 m using the same graduated cable for all well logs. The volume of investigation is a cylindrical shell of height 0.25 m, thickness 1–2 mm, and radius 6.5–7.6 cm, centered on the central axis of the tool (Walsh et al., 2013). The shallowest logged depth is 1.5 m, which is within bedrock and below soils in all boreholes. Measurements were acquired using two frequencies near 420 kHz and 480 kHz. We employed the minimum Dart pulse spacing of 0.5 ms, short (0.15 s) repolarization time, and a high running average of 168 stacks per measurement depth. Before each campaign, the tool system was calibrated in a shielded water sample in the lab. The NMR data were processed using commercial software (JavelinProcess_v4.4 and JavelinInterpret_v1.8, Vista Clara, Inc.). All stacks, stages, and frequencies associated with a measurement were combined, and the resulting NMR decay-curve was fit with a multiexponential decay function determined via a non-negative least squares inversion algorithm with second-order Tikhonov regularization using the default software regularization factor of 50. Water content estimated from our NMR measurements, θ_{nmr} ($\mathrm{m}^3/\mathrm{m}^3$), was taken as the value of the multiexpontential fit at time equals zero. Noise level was taken as the norm of the residuals after subtracting the multiexponential fit from the data.

Borehole neutron logs were acquired with two neutron gauges: a 501 neutron and gamma probe and a 503 moisture gauge (Instrotek, Concord, CA). Well log measurements were conducted for 25 s at depth increments of 0.30 m. The starting and ending depth of each survey varied between wells, depending on the height of casing stick up and the depth of the water table at the time of the survey. The volume of investigation is an ill-defined ellipsoid cloud centered on the probe (Bell, 1987). The linear calibration relation between neutron count, N, and water content, $\theta_{\mathrm{neutron}}$ ($\mathrm{m}^3/\mathrm{m}^3$), used for

501 measurements was developed by (Rempe & Dietrich, 2018) using a sand-packed barrel calibration for each borehole diameter. To allow for inter-probe comparison, this calibration was applied to the 501 by converting 501 counts to equivalent 503 count via linear regression of measurements acquired in locations in which water content is invariant (See SI, e.g. Ward et al., 2000; Ward & Wittman, 2009).

To obtain estimates of uncertainty in θ_{nmr} and $\theta_{\mathrm{neutron}}$, we performed repeat NMR and neutron measurements at different monitoring locations, using the same methods employed in logging measurements. Uncertainty was estimated as the mean standard deviation of all repeat measurement sets. The uncertainty in depth of the measurement was estimated as 0.5 cm.

Each borehole is associated with two sets of water content depth profiles: one derived from successive NMR logs and another derived from successive neutron logs obtained at roughly the same time. NMR and neutron measurements acquired at the same location at the same time are considered "paired" and allow for intra-method comparison of measurements. For each method, water content change, $\Delta\theta$ ($\mathrm{m}^3/\mathrm{m}^3$) is calculated as the difference in θ between wet and dry surveys. Dynamic storage, S_{dynamic} (mm), is calculated as the depth-integral of $\Delta\theta$, excluding locations where $\Delta\theta$ is not statistically different from zero (below uncertainty). The depth of dynamic storage is calculated as the depth at which the rate of increasing water content is lower than the rate of increasing uncertainty as $\Delta\theta$ is integrated from the surface. Total storage, S_{total} (mm), is calculated as the depth-integrated water content of the wettest, i.e. end-of-wet-season, condition. To account for differences in the vertical spacing of NMR and neutron measurements (0.3 m and 0.25 m respectively), we linearly interpolated θ_{nmr} and $\Delta\theta_{\mathrm{nmr}}$ and resampled the data at 0.25 m intervals.

3 Results

3.1 Water content measurement quality and uncertainty

We achieved high quality NMR decay-curves in unsaturated weathered bedrock. The mean noise level is nearly constant for all NMR measurements at 0.014 $\mathrm{m}^3/\mathrm{m}^3$ (standard deviation of 0.005 $\mathrm{m}^3/\mathrm{m}^3$). We find no correlation between noise level and θ_{nmr}, measurement location, or measurement date. In nearly all measurements (approximately 94%), signal is larger than noise such that the signal/noise ratio exceeds one. NMR sig-

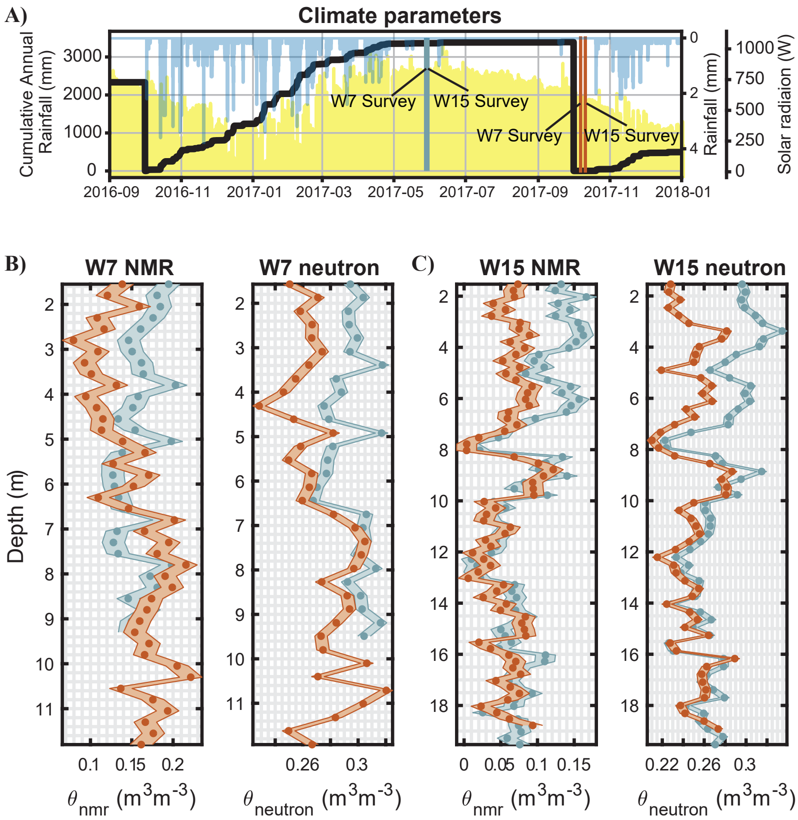

Figure 2. Example water content depth profiles which track the seasonal cycle of wetting and drying in the unsaturated zone of a thinly-soiled bedrock hillslope. Characteristic out-of-phase rainfall and solar radiation at Rivendell during the 2017 water year (A) drive deep water storage dynamics that are captured by successive well logging with NMR (θ_{nmr}) and neutron ($\theta_{\mathrm{neutron}}$) tools in W7 (B) and W15 (C) in May (blue) and October (orange) 2017. Well logging measurements are shown as discrete points and measurement uncertainty is shown as shaded envelopes. Overlapping envelopes between May and October measurements indicate that change in θ at that depth is below uncertainty.

nal amplitudes tend to decay rapidly—an average of 8 consecutive initial signal amplitudes are recorded per measurement before any single amplitude drops below noise level (e.g. Figure S2). Of the measurements reported here, 57% include at least five consecutive initial signal amplitudes above noise level.

Uncertainty in θ_{nmr} is estimated from repeat measurements. The standard deviation of repeat θ_{nmr} ranges from 0.002 to 0.024 m^3/m^3, with a mean of 0.014 m^3/m^3 (the standard deviation of repeat measurements is coincidentally the same as the mean noise level, Figure S3a). We take this mean as our estimate of θ_{nmr} uncertainty. The uncertainty in changes in water content between measurements, $\Delta\theta_{\mathrm{nmr}}$, is then 0.019 $\mathrm{m}^3/\mathrm{m}^3$. Among all monitoring measurements, θ_{nmr} ranges from 0.002 to 0.254 $\mathrm{m}^3/\mathrm{m}^3$ with a mean value of 0.078 $\mathrm{m}^3/\mathrm{m}^3$. Therefore, nearly all (96%) of θ_{nmr} measurements are larger than uncertainty.

Between wet and dry well logs, detectable differences in θ_{nmr} above uncertainty occur (Figure 2). Measurements of $\Delta\theta_{\mathrm{nmr}}$ range from -0.060 to 0.108 $\mathrm{m}^3/\mathrm{m}^3$ with a mean of 0.016 $\mathrm{m}^3/\mathrm{m}^3$. Only 31% of $\Delta\theta_{\mathrm{nmr}}$ measurements are larger than uncertainty, indicating that many of our monitoring locations either do not experience water content changes or changes are below detection (Figures 2 and 3). At shallow depths, differences in θ_{nmr} tend to be above uncertainty, while at deeper depths differences tend to be within uncertainty.

Uncertainty in $\theta_{\mathrm{neutron}}$ is estimated from repeat measurements. The standard deviation of $\theta_{\mathrm{neutron}}$ ranges from 0.001 to 0.013 $\mathrm{m}^3/\mathrm{m}^3$, with a mean of 0.005 $\mathrm{m}^3/\mathrm{m}^3$ (Figure S3b). We take this mean as our estimate of $\theta_{\mathrm{neutron}}$ uncertainty. The uncertainty in changes in water content between neutron measurements ($\Delta\theta_{\mathrm{neutron}}$) is then 0.006 $\mathrm{m}^3/\mathrm{m}^3$. Among all monitoring measurements, $\theta_{\mathrm{neutron}}$ ranges from 0.189 to 0.413 $\mathrm{m}^3/\mathrm{m}^3$ with a mean value of 0.256 $\mathrm{m}^3/\mathrm{m}^3$. All $\theta_{\mathrm{neutron}}$ values are greater than uncertainty.

Similar to NMR, differences in $\theta_{\mathrm{neutron}}$ tend to be above uncertainty at shallow depths and many monitoring locations did not show changes in water content (Figures 2 and 3). Change in water content, $\Delta\theta_{\mathrm{neutron}}$, ranges from -0.014 to 0.073 $\mathrm{m}^3/\mathrm{m}^3$ with a mean of 0.020 $\mathrm{m}^3/\mathrm{m}^3$. Of all $\Delta\theta_{\mathrm{neutron}}$ values, 23% are below the 0.006 $\mathrm{m}^3/\mathrm{m}^3$ uncertainty.

The magnitude of $\theta_{\mathrm{neutron}}$ is systematically higher than θ_{nmr} (Figures 2 and S3a), but there is agreement in $\Delta\theta$ for both measurement techniques (Figures 3 and S3b). The linear relationship ($\mathrm{R}^2 = 0.52$, $p \ll 0.01$) between paired θ_{nmr} and $\theta_{\mathrm{neutron}}$ measurements has a slope of nearly one (0.96 ± 0.03) with intercept 0.169 ± 0.7 $\mathrm{m}^3/\mathrm{m}^3$, indicating a systematic offset between otherwise approximately equivalent values. In the linear relationship between paired $\Delta\theta_{\mathrm{nmr}}$ and $\Delta\theta_{\mathrm{neutron}}$ measurements ($\mathrm{R}^2 = 0.30$, $p \ll 0.01$), the intercept vanishes (-0.42 ± 0.21), indicating that both methods are similarly sensitive to changes in water content.

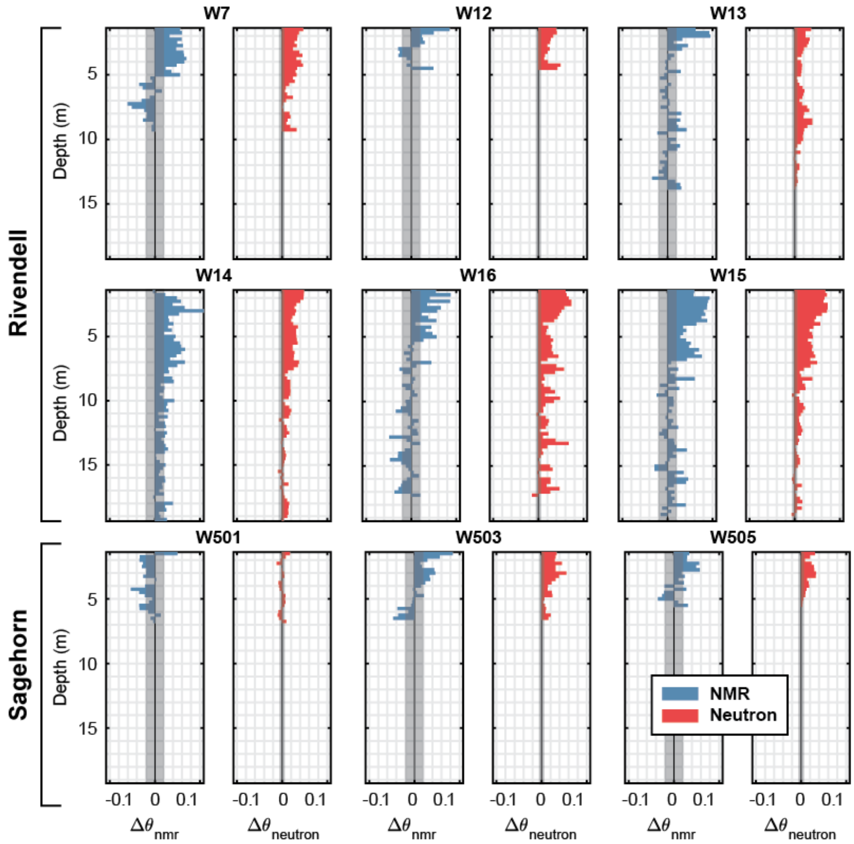

Figure 3. Water content change depth profiles measured with NMR ($\Delta\theta_{\mathrm{nmr}}$) and neutron ($\Delta\theta_{\mathrm{neutron}}$) well logs in the unsaturated zone of all study monitoring wells between May and October 2017 (See Table S1 for survey dates). The 68% confidence interval is depicted as grey vertical bars. $\Delta\theta$ values that lie within this interval are not considered significantly different than zero, and are not included in the calculation of dynamic storage.

3.2 Patterns of water content and dynamic storage

The spatial patterns of θ (Figure 2) and $\Delta\theta$ (Figure 3) resolved by NMR and neutron are consistent, despite the disagreement in the magnitude of θ_{nmr} and $\theta_{\mathrm{neutron}}$. Vertical profiles of θ_{nmr} and $\theta_{\mathrm{neutron}}$ show loss of vadose zone water storage between the start and end of the summer dry season. Over the dry season, θ generally decreases or does not change (Figure 3). However, for small values of $\Delta\theta_{\mathrm{neutron}}$ close to 0.01 m^3/m^3, the $\Delta\theta_{\mathrm{nmr}}$ is typically below detection and there are several depths where $\Delta\theta_{\mathrm{nmr}}$ and $\Delta\theta_{\mathrm{neutron}}$ have opposite signs. For example, at 7.5 m in W7, $\Delta\theta_{\mathrm{nmr}}$ is negative, while $\Delta\theta_{\mathrm{neutron}}$ is below detection (Figure 3).

The spatial variability in water storage among and within wells is captured by both methods consistently. Both NMR and neutron measurements of θ and $\Delta\theta$ are sensitive to features at the meter and sub-meter scale (Figures 2 and 3). For example, both θ_{nmr} and $\theta_{\mathrm{neutron}}$ in Figure 2C show an approximately 1 m thick interval of invariant, low water content centered at 7.7 m and and an approximately 1 m thick interval of dynamic, high water content centered at 3.3 m.

Storage estimates from NMR and neutron logging in this study are shown in Figure 4. With the exception of W16, S_{dynamic} estimates from NMR and neutron agree within uncertainty (Figure 4A and Table S2). In general, S_{dynamic} measured via neutron tends to be greater than S_{dynamic} measured via NMR (Figure 4A). This is due to the lower detection limit of neutron relative to NMR, such that small $\Delta\theta$ measurements are included in neutron S_{dynamic} estimates, but not NMR (Figure 3).

The spatial patterns of water storage are consistent with what has been recorded in previous years at these sites (Rempe & Dietrich, 2018; Hahm et al., Submitted). In particular, previous studies similarly report dynamic water storage concentrated at shallow depths in the unsaturated zone, with little dynamic storage occurring at depths that are above and within the zone where the water table fluctuates. (Table S1 lists the depths where groundwater is encountered.) Our 2017 S_{dynamic} measurements show general agreement with S_{dynamic} measured by successive neutron well logs conducted by Rempe and Dietrich (2018) and Hahm et al. (Submitted) during other water years, with the exception of W501 and W16. At W16, S_{dynamic} estimated via NMR is significantly lower than the S_{dynamic} measured by neutron in different years of observation. At W501, the discrepancy between S_{dynamic} measured in 2018 and 2017 is likely due to the timing of the

2018 survey, which occurred shortly after a rainfall event that transiently wetted the upper 1.5 m of the profile (Hahm et al., Submitted). Dralle et al. (2018) report catchment average S_{dynamic} of 380 ± 60 mm for Rivendell (Elder Creek watershed) and 90 ± 45 mm for Sagehorn (Dry Creek watershed) using a combination of streamflow recession analysis and hydrologic mass balance techniques. These S_{dynamic} estimates agree with the higher end of S_{dynamic} observed in our borehole measurements. Estimates of the depth of dynamic storage from NMR and neutron generally agree to within 2–3 m, with neutron estimates generally being less than NMR estimates due to the lower uncertainty of neutron measurements. Neutron estimates of S_{total} are roughly 2–5 times higher than NMR estimates due to θ_{neutron} being systematically greater than θ_{nmr}.

4 Discussion and conclusions

Successive borehole NMR measurements capture the timing, spatial pattern, and magnitude of water content changes in the bedrock vadose zone at two seasonally dry field sites. The agreement between NMR and neutron moderation indicates that borehole NMR is a reliable tool for monitoring dynamic storage in complex, heterogeneous bedrock vadose zones. We identify two important advantages to developing NMR for more widespread use in the deep vadose zone. First, there is great potential for linking NMR relaxation to hydraulic properties, such as water retention and hydraulic conductivity (e.g. Costabel & Yaramanci, 2011, 2013; Mohnke et al., 2014), which are otherwise exceptionally difficult to obtain in situ and at the field scale. This detailed hydraulic information can serve to mechanistically link the physical structure of unsaturated bedrock systems to watershed functioning (Brantley, Lebedeva, et al., 2017; Brantley, Eissenstat, et al., 2017; Riebe et al., 2017; Klos et al., 2018). Second, compared to neutron logging—the current standard for direct monitoring in unsaturated bedrock—NMR is not associated with regulatory burdens, NMR can be deployed from the surface as well as via borehole tools, and the NMR signal does not require a material-specific nor casing-specific calibration to arrive at water content. The comparative ease-of-use of borehole NMR should result in improved monitoring of flow and transport in the bedrock vadose zone for applications associated with critical zone biogeochemical cycling, landscape weathering, and ecohydrology.

The low precision (relatively high uncertainty) of θ_{nmr} presents the most significant limitation on the use of NMR in the bedrock vadose zone. The precision of our bore-

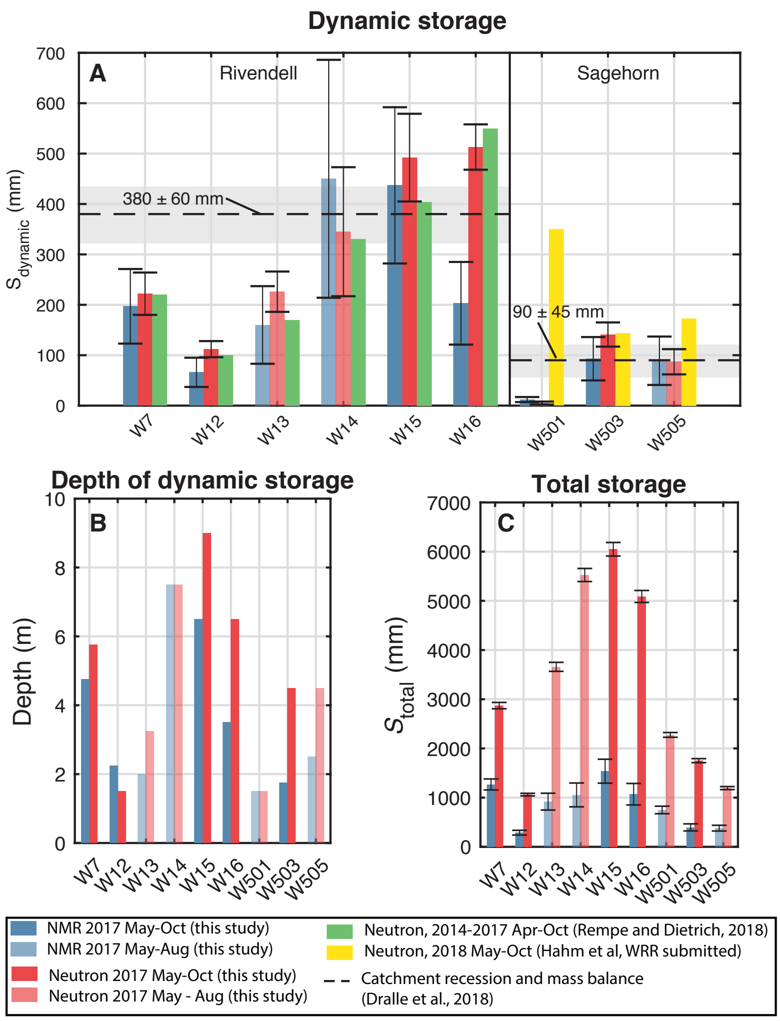

Figure 4. Comparison of dynamic storage (A), depth of dynamic storage (B), and total storage (C) from successive NMR (blue) and neutron (red) well logs. Error bars reflect the propagated uncertainty in θ and probe placement. Dynamic storage is calculated as the depth-integral of $\Delta\theta$ between profiles logged in the wettest (May 2017) and driest well logs (August 2017 for wells W13, W14, W501, W505, and October 2017 for wells W7, W12, W15, W16, W501). Dynamic storage estimated in other studies are shown for reference (Dralle et al., 2018; Hahm et al., Submitted). Depth of dynamic storage is the depth to which $\Delta\theta$ measurements are greater than measurement uncertainty. Total storage is calculated as the depth integral of water content measured in the May well logs, which represent wet conditions.

hole θ_{nmr} measurements (± 0.014 m^3/m^3) based on repeat measurements is on the order of other water content measurement techniques such as TDR (Roth et al., 1990). Our uncertainty estimate is specific to this study because it represents acquisition parameters, processing settings, and the specific field conditions of this study. In many monitoring locations, water content changes that were undetectable with NMR were detectable with neutron, which limits the extent to which water content measurements can be compared over space and time. In one monitoring location (W16), this discrepancy resulted in an underestimate of S_{dynamic} from NMR relative to neutron (Figure 4). In spite of the limitations of NMR precision, our well logs led to reliable estimates of dynamic storage, suggesting that NMR could be applied reliably to a broad range of rock types and settings.

Several strategies could be considered to achieve higher precision estimates of dynamic storage with NMR. Uncertainty in θ_{nmr} is derived primarily from the multi-exponential fit to the NMR decay-curve. The estimate of θ_{nmr} is in principle independent of relaxation and is dependant only on the initial amplitude of the decay-curve, but in practice θ is often estimated from the initial value of the multi-exponential fit. This fit-derived θ can be larger than the initial decay-curve amplitude if a significant fraction of water content is characterized by low relaxation times relative to the tool's pulse spacing time. In the vadose zone, water contents and relaxation times can be can be low, resulting in noisy, short decay-curves that inherently lead to uncertainty in θ_{nmr}. To combat these sources of uncertainty, a high running average and low logging speed can be applied to arrive at sufficiently high signal/noise ratio for monitoring small changes in low water contents. Additionally, logging speed can be improved by using short repolarization times and measurement lengths. To address variations in relaxation in space and time within a given well log, we recommend initiating well logs with repeat measurements at representative locations and tuning logging parameters based on these site- and timing-specific results. Another possible contribution to uncertainty is incorrect probe placement in the field. Small movements in the probe between or within measurements could be particularly important in fractured bedrock environments, because small changes in the position of the sensitive shell could drastically change the volume of water that intersects the shell.

While there is agreement in $\Delta\theta$ between paired NMR and neutron measurements, we identify a systematic difference between estimates of θ_{nmr} and $\theta_{\mathrm{neutron}}$ that leads to a large systematic difference in estimates of S_{total} between methods (Figure 4). The systematic difference between estimates of θ_{nmr} and θ_{neutron} is likely attributable to two non-mutually-exclusive mechanisms: (i) θ_{nmr} is a systematic underestimate due to the presence of a large volume of seasonally invariant water content that is invisible to NMR due to low relaxation times below the detection limit of the tool, and (ii) θ_{neutron} does not accurately capture in situ θ due to issues with the calibration relationship between θ and neutron counts. Because factors that affect the NMR signal in the vadose zone tend to decrease θ_{nmr} relative to θ, it is reasonable to suggest that S_{total} estimated from NMR sets a lower bound on true total storage. We note that besides the broad systematic offset, the relationship between θ_{nmr} vs θ_{neutron} appears to vary with borehole location (Figure S4), suggesting that variability in in-situ chemical composition and bulk density of the bedrock is poorly represented by the calibration relationship between θ_{neutron} and neutron counts. While there is uncertainty about the magnitude of S_{total}, the non-zero end-of-dry-season water content documented by NMR logging provides evidence for a substantial volume of non-dynamic storage in the bedrock vadose zone. This non-dynamic storage has implications for water mixing and water-rock interactions.

There is considerable agreement between the spatiotemporal patterns of dynamic storage resolved by our NMR and neutron measurements. Both methods show that dynamic storage is concentrated at shallow depths, and we propose that the depth of dynamic storage (Figure 4) could represent an effective rooting depth. All or most of the dynamic storage reported here likely supplies transpiration for woody vegetation (Rempe & Dietrich, 2018; Dralle et al., 2018; Hahm et al., Submitted). At both sites, roots in bedrock are observed in exposures (Rempe & Dietrich, 2018; Hahm et al., 2019), and at Rivendell, roots were observed to 16 m when drilling. The depth of dynamic storage is variable across the sites (Figure 4) such that neither site can be characterized by a single effective rooting depth. Patterns of dynamic storage diverge between methods at depths below the depth of dynamic storage where small changes occur that do not contribute significantly to dynamic storage.

The bedrock vadose zone at our sites is highly fractured, and we propose that dynamic storage is dominantly if not exclusively held in fractures. Given that pore diameters in the fine-grained matrix of our site are largely at the micron-scale (Gu et al., 2020; Hahm et al., 2018), exceptionally low (negative) water potential would be needed to remove water from bedrock matrix pores, and water held in much of the matrix is likely to be characterized by relaxation times below the 1 ms pulse spacing time of the Dart (e.g. Lewis et al., 2013). Nonetheless, we note that NMR detects both dynamic and non-dynamic pore domains because there is non-zero θ_{nmr} at the end of the dry season. The pores experiencing seasonal water gain and loss are larger and more interconnected than the pores storing non-dynamic water, and likely include water stored within fractures. For the assumption that dynamic storage occurs exclusively within fractures, the range of $\Delta\theta$ of 0.108 $\mathrm{m}^3/\mathrm{m}^3$ (Figure 3) would represent the minimum fracture porosity. Future studies could use NMR relaxation measurements with measurements of surface relaxivity to evaluate the sizes and shapes of pores which host seasonally dynamic water (e.g. Mohnke et al., 2014).

Acknowledgments

The authors thank the University of California Angelo Coast Range Reserve, the University of California reserve system, and Marilyn and Jerry Russell and the Holleman family and for land access. This research was funded by the US Department of Energy, Office of Science, Office of Biological Environmental Research under award number DESC0018039 and the National Science Foundation supported Eel River Critical Zone Observatory (NSF EAR 1331940). The authors thank Nicholas Soto-Kerans, Colt Kernan, Zach Mungia, Mariel Nelson, Amy De Luna, Brandon Minton, and Peter Steel for conducting or facilitating field work. Data from the Eel River Critical Zone Observatory used in this publication are available at https://sensor.berkeley.edu/. Data and the results presented in this study can be obtained through Hydroshare at

https://www.hydroshare.org/resource/a84d6530dc8c43f69402e448969f3a89/

References

Babaeian, E., Sadeghi, M., Jones, S. B., Montzka, C., Vereecken, H., & Tuller, M. (2019). Ground, proximal, and satellite remote sensing of soil moisture. *Reviews of Geophysics*, *57*, 530–616.

Behroozmand, A. A., Keating, K., & Auken, E. (2015). A review of the principles and applications of the NMR technique for near-surface characterization. *Surveys in geophysics*, *36*, 27–85.

Bell, J. (1987). Neutron probe practice.

Brantley, S. L., Eissenstat, D. M., Marshall, J. A., Godsey, S. E., Balogh-Brunstad, Z., Karwan, D. L., . . . others (2017). Reviews and syntheses: on the roles trees play in building and plumbing the critical zone. *Biogeosciences (Online)*, *14*.

Brantley, S. L., Lebedeva, M. I., Balashov, V. N., Singha, K., Sullivan, P. L., & Stinchcomb, G. (2017). Toward a conceptual model relating chemical reaction fronts to water flow paths in hills. *Geomorphology*, *277*, 100–117.

Carrière, S. D., Chalikakis, K., Danquigny, C., Davi, H., Mazzilli, N., Ollivier, C., & Emblanch, C. (2016). The role of porous matrix in water flow regulation within a karst unsaturated zone: an integrated hydrogeophysical approach. *Hydrogeology Journal*, *24*, 1905–1918.

Costabel, S., & Yaramanci, U. (2011). Relative hydraulic conductivity in the vadose zone from magnetic resonance sounding—Brooks-Corey parameterization of the capillary fringe. *Geophysics*, *76*, G61–G71.

Costabel, S., & Yaramanci, U. (2013). Estimation of water retention parameters from nuclear magnetic resonance relaxation time distributions. *Water resources research*, *49*, 2068–2079.

Dralle, D. N., Hahm, W. J., Rempe, D. M., Karst, N. J., Thompson, S. E., & Dietrich, W. E. (2018). Quantification of the seasonal hillslope water storage that does not drive streamflow. *Hydrological processes*, *32*, 1978–1992.

Faybishenko, B., Doughty, C., Steiger, M., Long, J. C., Wood, T. R., Jacobsen, J. S., . . . Zawislanski, P. T. (2000). Conceptual model of the geometry and physics of water flow in a fractured basalt vadose zone. *Water resources research*, *36*, 3499–3520.

Flinchum, B. A., Holbrook, W. S., Grana, D., Parsekian, A. D., Carr, B. J., Hayes, J. L., & Jiao, J. (2018). Estimating the water holding capacity of the critical zone using near-surface geophysics. *Hydrological Processes*, *32*, 3308–3326.

Flinchum, B. A., Holbrook, W. S., Parsekian, A. D., & Carr, B. J. (2019). Characterizing the critical zone using borehole and surface nuclear magnetic resonance. *Vadose Zone Journal*, *18*.

Gu, X., Rempe, D. M., Dietrich, W. E., West, A. J., Lin, T.-C., Jin, L., & Brantley, S. L. (2020). Chemical reactions, porosity, and microfracturing in shale during weathering: The effect of erosion rate. *Geochimica et Cosmochimica Acta*, *269*, 63–100.

Gwo, J.-P., Jardine, P. M., & Sanford, W. (2005). Effect of advective mass transfer on field scale fluid and solute movement: Field and modeling studies at a waste disposal site in fractured rock at Oak Ridge National Laboratory, Tennessee, USA. *Hydrogeology journal*, *13*, 565–583.

Hahm, W. J., Dietrich, W. E., & Dawson, T. E. (2018). Controls on the distribution and resilience of Quercus garryana: ecophysiological evidence of oak's water-limitation tolerance. *Ecosphere*, *9*, e02218.

Hahm, W. J., Dralle, D. N., Rempe, D. M., Bryk, A. B., Thompson, S. E., Dawson, T. E., & Dietrich, W. E. (2019). Low subsurface water storage capacity relative to annual rainfall decouples Mediterranean plant productivity and water use from rainfall variability. *Geophysical Research Letters*, *46*, 6544–6553.

Hahm, W. J., Rempe, D. M., Dralle, D. N., Dawson, T. E., & Dietrich, W. E. (Submitted). Oak transpiration drawn from the weathered bedrock vadose zone in the summer dry season. *Water resources research*.

Hansen, M. C., Potapov, P. V., Moore, R., Hancher, M., Turubanova, S. A., Tyukavina, A., ... others (2013). High-resolution global maps of 21st-century forest cover change. *science*, *342*, 850–853.

Ireson, A., Mathias, S., Wheater, H., Butler, A., & Finch, J. (2009). A model for flow in the chalk unsaturated zone incorporating progressive weathering. *Journal of Hydrology*, *365*, 244–260.

Jayko, A., Blake, M., McLaughlin, R., Ohlin, H., Ellen, S., & Kelsey, H. (1989). *Reconnaissance geologic map of the covelo 30-by 60-minute quadrangle, northern california* (Tech. Rep.). US Government Printing Office.

Keating, K., & Knight, R. (2008). A laboratory study of the effect of magnetite on NMR relaxation rates. *Journal of Applied Geophysics*, *66*, 188–196.

Keating, K., & Knight, R. (2010). A laboratory study of the effect of Fe (II)-bearing minerals on nuclear magnetic resonance (NMR) relaxation measurements. *Geophysics*, *75*, F71–F82.

Klos, P. Z., Goulden, M. L., Riebe, C. S., Tague, C. L., O'Geen, A. T., Flinchum, B. A., ... others (2018). Subsurface plant-accessible water in mountain ecosystems with a Mediterranean climate. *Wiley Interdisciplinary Reviews: Water*, *5*, e1277.

Lesparre, N., Girard, J.-F., Jeannot, B., Weill, S., Dumont, M., Boucher, M., ... Delay, F. (2020). Magnetic resonance sounding measurements as posterior information to condition hydrological model parameters: Application to a hard-rock headwater catchment. *Journal of Hydrology*, 124941.

Lewis, R., Singer, P., Jiang, T., Rylander, E., Sinclair, S., Mclin, R. H., et al. (2013). NMR T2 distributions in the eagle ford shale: reflections on pore size. In *Spe unconventional resources conference-usa.*

Mohnke, O., Nordlund, C., Jorand, R., & Klitzsch, N. (2014). Understanding NMR relaxometry of partially water-saturated rocks. *Hydrology and Earth System Sciences Discussions*, *11*, 12697–12729.

PRISM Climate Group. (2004). *Oregon state university.* (data retrieved from `http://prism.oregonstate.edu`, created Feb 4, 2004)

Rempe, D. M., & Dietrich, W. E. (2018). Direct observations of rock moisture, a hidden component of the hydrologic cycle. *Proceedings of the National Academy of Sciences*, *115*, 2664–2669.

Rempe, D. M., Schmidt, L. M., & Hahm, W. J. (2018). In-situ nuclear magnetic resonance detection of fracture-held water in variably saturated bedrock. In *Seg technical program expanded abstracts 2018* (pp. 4919–4923). Society of Exploration Geophysicists.

Riebe, C. S., Hahm, W. J., & Brantley, S. L. (2017). Controls on deep critical zone architecture: A historical review and four testable hypotheses. *Earth Surface Processes and Landforms*, *42*, 128–156.

Roth, K., Schulin, R., Flühler, H., & Attinger, W. (1990). Calibration of time domain reflectometry for water content measurement using a composite dielectric approach. *Water Resources Research*, *26*, 2267–2273.

Salve, R., Rempe, D. M., & Dietrich, W. E. (2012). Rain, rock moisture dynamics, and the rapid response of perched groundwater in weathered, fractured argillite underlying a steep hillslope. *Water Resources Research*, *48*.

Schwinning, S. (2010). The ecohydrology of roots in rocks. *Ecohydrology: Ecosystems, Land and Water Process Interactions, Ecohydrogeomorphology*, *3*, 238–245.

Walsh, D., Turner, P., Grunewald, E., Zhang, H., Butler Jr, J. J., Reboulet, E., … others (2013). A small-diameter NMR logging tool for groundwater investigations. *Groundwater*, *51*, 914–926.

Wan, J., Tokunaga, T. K., Williams, K. H., Dong, W., Brown, W., Henderson,

A. N., ... Hubbard, S. S. (2019). Predicting sedimentary bedrock subsurface weathering fronts and weathering rates. *Scientific reports*, *9*, 1–10.

Ward, A. L., Caldwell, T. G., & Gee, G. W. (2000). *Vadose zone transport field study: Soil water content distributions by neutron moderation* (Tech. Rep.). Pacific Northwest National Lab.(PNNL), Richland, WA (United States).

Ward, A. L., & Wittman, R. S. (2009). *Calibration of a neutron hydroprobe for moisture measurements in small-diameter steel-cased boreholes* (Tech. Rep.). Pacific Northwest National Lab.(PNNL), Richland, WA (United States).

Supporting Information for "Quantifying dynamic water storage in unsaturated bedrock with borehole nuclear magnetic resonance"

Logan Schmidt[1], Daniella Rempe[1]

[1]Department of Geological Sciences, Jackson School of Geosciences, University of Texas at Austin, Austin, TX 78701

Contents of this file

Measurement of water content with neutron moderation

Two neutron probe instruments were used to monitor water content in this study: a 503 moisture gauge and a 501 neutron and gamma probe (Instrotek, Concord, CA). Each instrument requires a characteristic calibration to convert neutron count, N, to volumetric water content, θ. A linear calibration relationship was developed for the 503 instrument by Rempe and Dietrich (2018) using sand-packed barrels for each of the two PVC casing diameters used to line the boreholes at the site. The 503 measurements made in this study

---

Corresponding author: L. Schmidt, Department of Geological Sciences, Jackson School of Geosciences, University of Texas at Austin, Austin, TX 78701 (loganmschmidt@utexas.edu)

were obtained after the 503 instrument was serviced, necessitating a new calibration. To use the calibration developed for the pre-servicing 503 instrument for measurements taken after servicing with the same instrument, a linear equation was developed to convert post-servicing 503 N to equivalent pre-servicing N. To to this, we used over 6 years of moisture monitoring with pre-servicing 503 instrument and over 2 years of moisture monitoring post-servicing, and identified 26 monitoring locations at our sites (depths in monitoring boreholes) where (i) at least 5 measurements with each instrument had been made and (ii) water content values were nearly constant. A location satisfies (ii) and is considered invariant when the standard deviation of N at that location is less than or equal to the first quartile of all measurements. A linear relation between the mean pre-servicing N and mean post-servicing N measured at each of the 26 invariant locations was determined via least-squares regression. The same procedure was employed to convert N measured with the 501 instrument (2 years of monitoring) to equivalent pre-servicing 503 N. We identified 46 monitoring locations to establish the linear relationship. The data and two equations used to convert post-servicing 503 N and 501 N to equivalent pre-servicing 503 N are shown in Figure S1.

References

Rempe, D. M., & Dietrich, W. E. (2018). Direct observations of rock moisture, a hidden component of the hydrologic cycle. *Proceedings of the National Academy of Sciences*, *115*(11), 2664–2669.

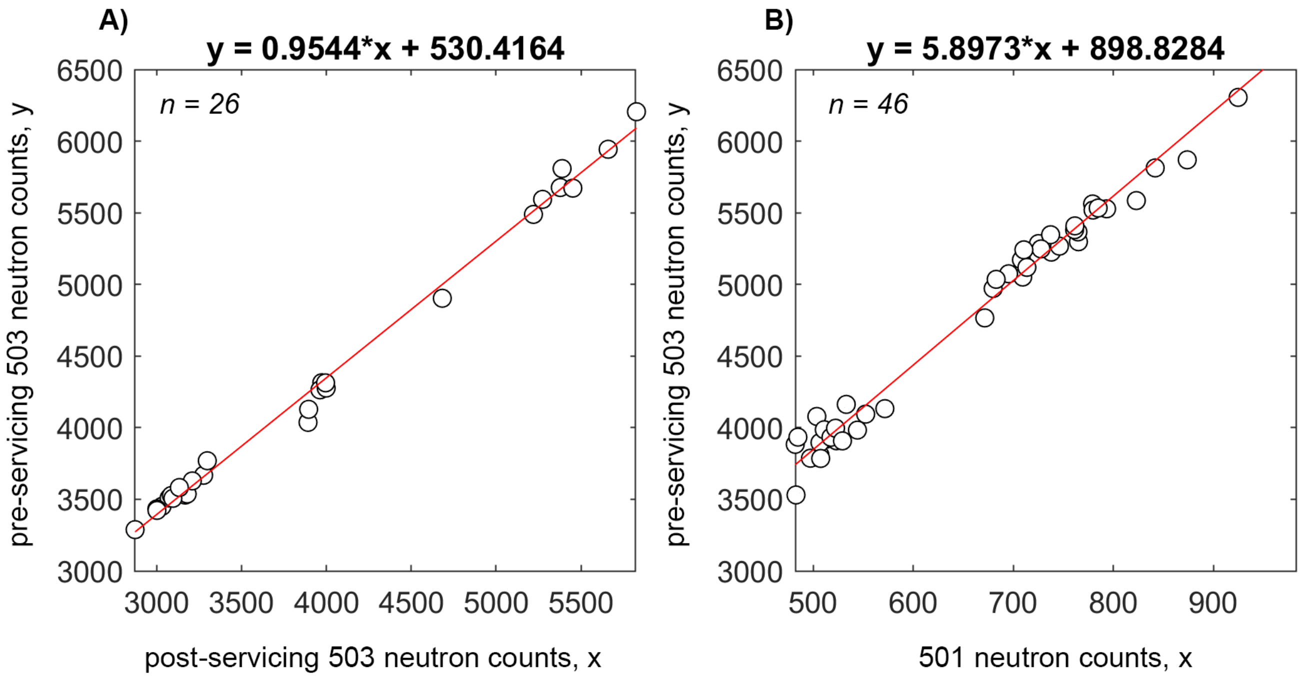

Figure S1. Data and equations used to convert neutron counts, N, measured by instruments in this study to equivalent counts made by the instrument used by Rempe and Dietrich (2018). Two conversions were developed: one for the 503 moisture gauge for N measured after the instrument was serviced (A), and one for the 501 neutron and gamma probe (B). Data represent the mean water content measured at monitoring locations at our study sites where water content has been found to be nearly constant across several years of monitoring. The superimposed red line represents the linear least-squares relation used to convert neutron counts. The number of data used in the regression is shown in the upper left.

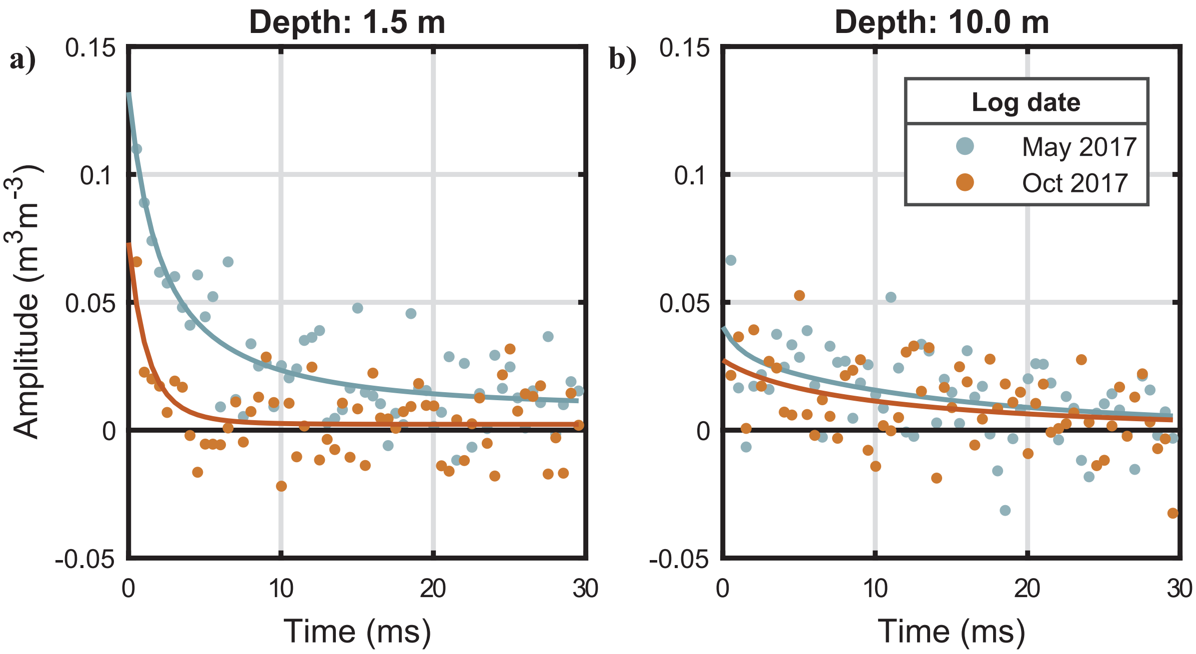

Figure S2. The effect of drying on the NMR decay-curve is shown for measurements made at 1.5 m depth (a) and 10.0 m depth (b) in a bedrock vadose zone at Rivendell in W15. Individual NMR decay amplitudes—scaled to units of volumetric water content—are shown as discrete points, and superimposed curves are the multi-exponential fit to these values. The value of the fit at time zero is θ_{nmr} for that measurement.

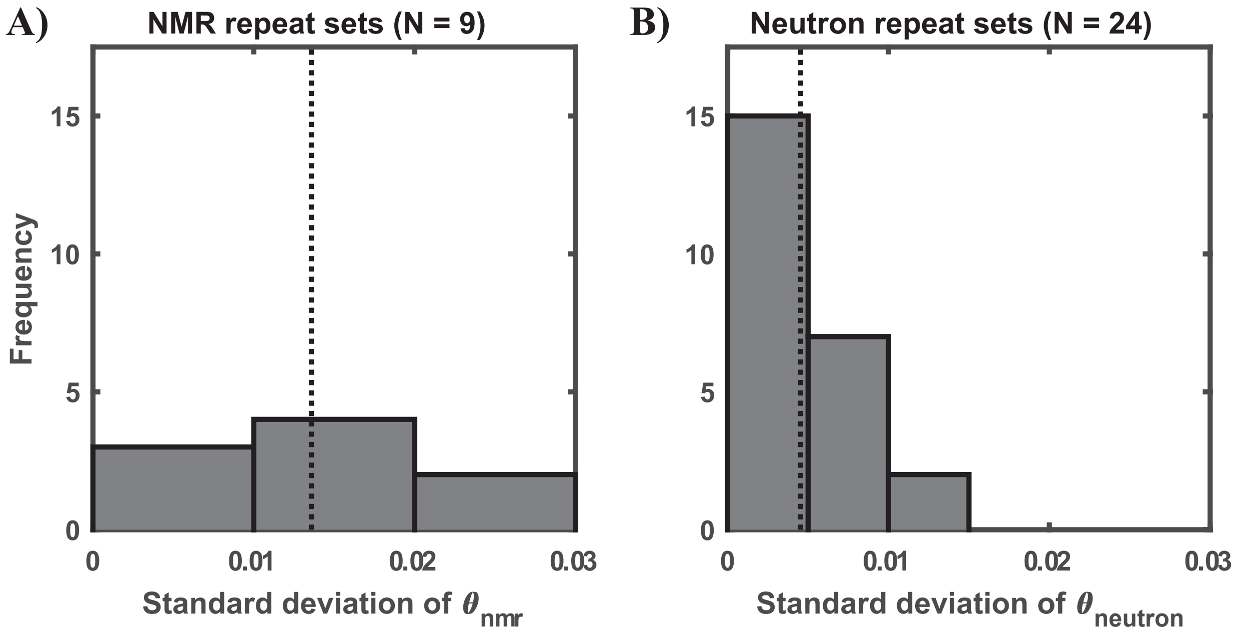

Figure S3. The distribution of standard deviation values of water content estimates obtained in repeat measurement sets using NMR (A) and neutron tools (B). In each panel, the dotted black vertical line indicates the mean standard deviation of all repeat sets which we take as measurement uncertainty.

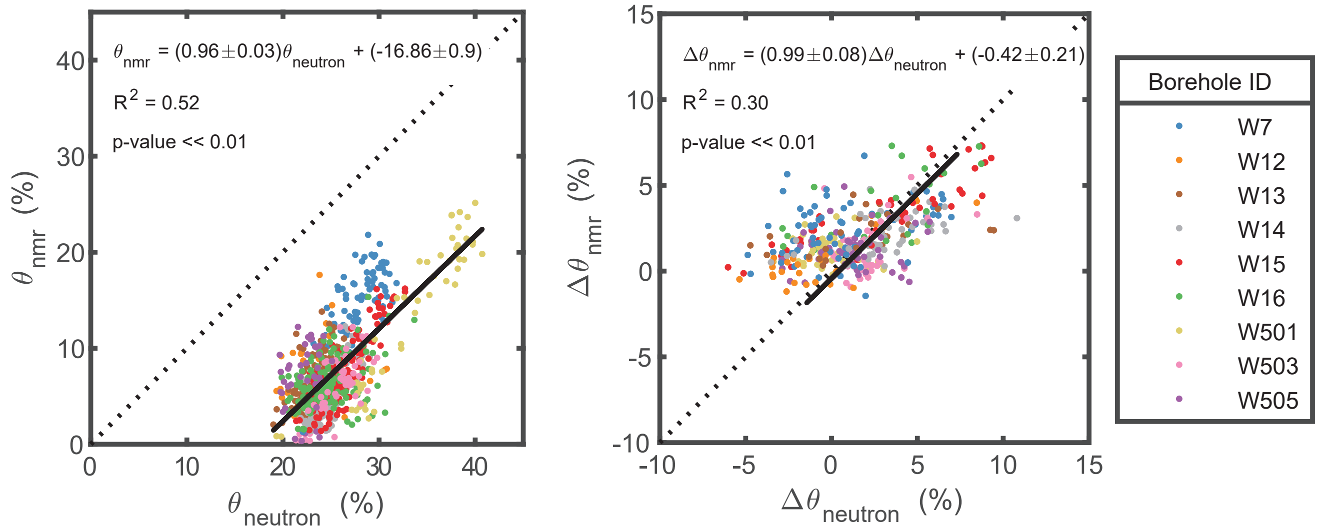

Figure S4. The relationship for θ and $\Delta\theta$ between paired NMR and neutron measurements. Color corresponds to borehole location, the solid black line is the linear least-squares fit to the data, and the dotted line is the one-to-one line.

Table S1. Borehole information

Site	Well ID	Wellhead elevation (m)	Well depth (m)	Well diameter (in)	Water table min depth (m)	Water table max depth (m)	Date of early-dry-season log (NMR)	Date of late-dry-season log (NMR)	Date of early-dry-season log (Neutron)	Date of late-dry-season log (Neutron)
Rivendell	W7	454	19.8	2	3.9	5.8	2017-05-28	2017-10-11	2017-05-28	2017-10-08
Rivendell	W12	402	7.2	2	3.3	5.9	2017-05-24	2017-10-10	2017-05-29	2017-10-08
Rivendell	W13	420	18.4	2	14.2	17.3	2017-05-09	2017-08-13	2017-05-28	2017-08-11
Rivendell	W14	445	32.9	3	8.2	28.1	2017-05-29	2017-08-12	2017-05-28	2017-08-11
Rivendell	W15	468	33.2	3	19.2	26.4	2017-05-30	2017-10-07	2017-05-14	2017-10-10
Rivendell	W16	455	34.3	3	11.1	23.2	2017-05-24	2017-10-07	2017-05-30	2017-10-10
Sagehorn	W501	712	15.27	3	2.6	9.9	2017-05-25	2017-08-15	2017-05-26	2017-08-17
Sagehorn	W503	722	10.21	3	5.6	8.3	2017-05-25	2017-10-13	2017-05-26	2017-10-09
Sagehorn	W505	722	6.28	2	Dry	Dry	2017-05-25	2017-08-17	2017-05-26	2017-08-17

Table S2. Storage estimates derived from NMR and neutron logging in each borehole.

Well ID	NMR depth of dynamic storage (m)	Neutron depth of dynamic storage (m)	NMR dynamic storage (mm)	Neutron dynamic storage (mm)	NMR total storage (mm)	Neutron total storage (mm)
W7	4.8	5.8	197 ± 74	222 ± 42	1268 ± 112	2871 ± 65
W12	2.3	1.5	66 ± 29	112 ± 16	287 ± 48	1062 ± 26
W13	2.0	3.3	160 ± 77	226 ± 40	919 ± 171	3658 ± 92
W14	7.5	7.5	450 ± 236	345 ± 128	1055 ± 242	5525 ± 133
W15	6.5	9.0	437 ± 155	492 ± 87	1537 ± 243	6048 ± 138
W16	3.5	6.5	203 ± 82	513 ± 45	1069 ± 219	5089 ± 122
W501	1.5	1.5	12 ± 5	5 ± 3	749 ± 77	2275 ± 48
W503	1.8	4.5	93 ± 43	141 ± 24	395 ± 72	1752 ± 41
W505	2.5	4.5	89 ± 48	87 ± 25	380 ± 58	1194 ± 31